8-1998

Parity Nonconservation in Neutron Resonances in 232Th,

Sharon L. Stephenson
Gettysburg College

J D. Bowman
Los Alamos National Laboratory

Bret E. Crawford
Gettysburg College

See next page for additional authors

Stephenson, S., Bowman, J. D., Crawford, B .E., Delheij, P. P. J., Frankle, C. M., IInuma, M., Knudsen, J. N., Lowie, L. Y., Masaike, A., Matsuda, Y., Mitchell, G. E., Penttila, S. I., Postma, H., Roberson, N. R., Seestrom, S. J., Sharapov, E. I., Yen, Y.-F., and Yuan, V. W. (1998). Parity Nonconservation in Neutron Resonances in 232Th. Physical Review C, 58(2), 1236–1246. http://dx.doi.org/10.1103/PhysRevC.58.1236

Parity Nonconservation in Neutron Resonances in 232Th,

Abstract

Parity nonconservation (PNC) was measured for 24 p-wave resonances from 8 to 300 eV in ^{232}Th by measuring the helicity dependence of the total neutron cross section for epithermal neutrons with an improved experimental system. Ten resonances show statistically significant parity violation. For these ten resonances the analyzing powers are all positive, thus confirming the previously observed sign correlation. The data are fit to the sum of two terms, a constant asymmetry and a fluctuating asymmetry. With this ansatz the root-mean-square PNC matrix element M=1.12 meV, which corresponds to a weak spreading widthΓ_w=4.7×10^{-7} eV. For the neighboring nuclide ^{238}U there is no constant offset, suggesting that the sign correlation is specific to ^{232}Th.

Disciplines

Atomic, Molecular and Optical Physics | Physics

Authors

Sharon L. Stephenson, J D. Bowman, Bret E. Crawford, P P J. Delheij, C M. Frankle, M IInuma, J N. Knudsen, L Y. Lowie, A Masaike, Y Matsuda, G E. Mitchell, S I. Penttila, H Postma, N R. Roberson, S J. Seestrom, E I. Sharapov, Y-F Yen, and V W. Yuan

Parity nonconservation in neutron resonances in ^{232}Th

S. L. Stephenson,[1,*] J. D. Bowman,[2] B. E. Crawford,[3,†] P. P. J. Delheij,[4] C. M. Frankle,[2] M. Iinuma,[5,‡] J. N. Knudson,[2] L. Y. Lowie,[1,§] A. Masaike,[5] Y. Matsuda,[5] G. E. Mitchell,[1] S. I. Penttilä,[2] H. Postma,[6] N. R. Roberson,[3] S. J. Seestrom,[2] E. I. Sharapov,[7] Y.-F. Yen,[2,‖] and V. W. Yuan[2]

[1]*North Carolina State University, Raleigh, North Carolina 27695-8202*
and Triangle Universities Nuclear Laboratory, Durham, North Carolina 27708-0308
[2]*Los Alamos National Laboratory, Los Alamos, New Mexico 87545*
[3]*Duke University, Durham, North Carolina 27708*
and Triangle Universities Nuclear Laboratory, Durham, North Carolina 27708-0308
[4]*TRIUMF, Vancouver, British Columbia, Canada V6T 2A3*
[5]*Department of Physics, Kyoto University, Kyoto 606-8502, Japan*
[6]*University of Technology, Delft, 2600 GA, The Netherlands*
[7]*Joint Institute for Nuclear Research, 141980 Dubna, Russia*

(Received 6 April 1998)

Parity nonconservation (PNC) was measured for 24 p-wave resonances from 8 to 300 eV in ^{232}Th by measuring the helicity dependence of the total neutron cross section for epithermal neutrons with an improved experimental system. Ten resonances show statistically significant parity violation. For these ten resonances the analyzing powers are all positive, thus confirming the previously observed sign correlation. The data are fit to the sum of two terms, a constant asymmetry and a fluctuating asymmetry. With this ansatz the root-mean-square PNC matrix element $M=1.12$ meV, which corresponds to a weak spreading width $\Gamma_w=4.7\times10^{-7}$ eV. For the neighboring nuclide ^{238}U there is no constant offset, suggesting that the sign correlation is specific to ^{232}Th. [S0556-2813(98)03608-5]

PACS number(s): 25.40.Ny, 24.80.+y, 11.30.Er, 27.90.+b

I. INTRODUCTION

As discussed in the preceding paper [1], the traditional approach to symmetry breaking in the nucleus is illustrated by the study of parity nonconservation (PNC) in parity doublets in light nuclei. The classic review of PNC studies in light nuclei is by Adelberger and Haxton [2]. After the discovery [3] of very large enhancements of parity violation for neutron resonances in heavy nuclei (as large as 10^6), an approach was adopted that considers the compound nucleus as a chaotic system and treats the symmetry-breaking matrix elements as random variables. The experimental goal of the parity-violation experiments is the determination of the root-mean-square PNC matrix element. Recent reviews that adopt the approach include Bowman *et al.* [4], Frankle *et al.* [5], and Flambaum and Gribakin [6].

Initial measurements by the TRIPLE Collaboration produced a number of parity violations in ^{238}U [7,8] and ^{232}Th [9,10], and raised several questions. Of particular interest was the unexpected nonstatistical result observed in ^{232}Th [9,10]: all seven statistically significant asymmetries have the same sign. This result generated a large amount of interest and theoretical speculation. It was considered very important to repeat the measurements on thorium with improved precision in order to verify the anomaly. It was also important to learn whether the effect is universal or specific to ^{232}Th.

We made significant improvements to the experimental system, and repeated the measurements for ^{238}U and ^{232}Th. The new data were analyzed with an improved analysis procedure. This paper and the preceding paper on ^{238}U report the results of these measurements. Details of the ^{232}Th experiment, analysis, and results are presented in the dissertation of Stephenson [11].

The spirit of the analysis is the same as in the preceding paper. The PNC asymmetry p for a p-wave resonance is obtained from $\sigma_p^{\pm}=\sigma_p\ (1+p^{\pm})$, where $\sigma_p^{\pm}$ is the resonance cross section for $+$ and $-$ helicities, and σ_p is the resonance part of the p-wave cross section. (Here the neutron polarization is assumed to be one for simplicity. In the data analysis the measured polarization value was included in the determination of the longitudinal asymmetry.) The resonance parameters are determined (with the multilevel, multichannel code described in the preceding paper) from summed data obtained under similar conditions. The resonance parameters are then held fixed, including the resonance cross section σ_p for the p-wave resonance in question, and the longitudinal asymmetries are determined separately for the $+$ and $-$ helicity states. The asymmetry parameters $p^{\pm}$ are obtained from $\sigma_p^{\pm}$, and the longitudinal asymmetry p determined

*Present address: Gettysburg College, Gettysburg, PA 17325.
†Present address: North Carolina State University, Raleigh, NC 27695-8202 and Gettysburg College, Gettysburg, PA 17325.
‡Present address: Hiroshima University, Hiroshima-Ken 739-8526, Japan.
§Present address: McKinsey and Company, Atlanta, GA 30303.
‖Present address: Wake Forest University School of Medicine, Winston-Salem, NC 27157.

from $p=(\sigma_p^+-\sigma_p^-)/(\sigma_p^++\sigma_p^-)=(p^+-p^-)/(2+p^++p^-)$.

The apparatus is described briefly in Sec. II, while Sec. III discusses the procedure used to obtain the resonance parameters and the longitudinal asymmetries. The data set is described in Sec. IV. The results—resonance parameters and PNC longitudinal asymmetries—are presented in Sec. V. The analysis used to obtain the rms PNC matrix element from the asymmetries is described in Sec. VI. The sign correlation is discussed in Sec. VII and a brief summary is given in the final section.

II. EXPERIMENTAL METHOD

A. Apparatus

Since the apparatus is described in detail in the preceding paper, here we only summarize the major parts of the system. The 800-MeV proton beam from the Los Alamos Neutron Scattering Center (LANSCE) linac is chopped to pulses 250-ns wide, which are stacked on top of one another and accumulated in the Proton Storage Ring (PSR). The stored proton beam (typically the average proton current was 60 μ for this experiment) is then directed at the rate of 20 Hz towards a tungsten spallation target and approximately 17 fast neutrons in the MeV energy range are produced for each incident proton. The neutrons are then moderated to epithermal energies in a gadolinium-poisoned water moderator and collimated. The resulting pulsed, intense epithermal neutron beam at the Manuel Lujan Neutron Scattering Center (MLNSC) is well suited for these PNC experiments. A detailed description of the target-moderator geometry is given by Lisowski *et al.* [12]. In addition to the initial width that the neutron pulse acquires from the proton pulse, further broadening is introduced by the neutron moderation process.

A description of the TRIPLE Collaboration experimental setup as utilized in the original experiment on ^{232}Th was given by Roberson *et al.* [13]. Although major changes have been made to most of the system, the overall experimental philosophy remains the same. An overview of the TRIPLE experimental system is shown in Fig. 1.

The neutron flux is monitored by a pair of ionization chambers [14]. The neutron beam is polarized by transmission through a polarized proton target. The protons are polarized in frozen ammonia by the dynamic nuclear polarization process [15,16]. The ammonia target is cooled in liquid ^{4}He to 1 K at the center of a 5-T split-coil superconducting magnet. The proton polarization was monitored with a nuclear magnetic resonance (NMR) measurement. The NMR measurement provides a rapid *relative* determination of the proton polarization. Calibration methods of the polarization are discussed by Yuan *et al.* [17]. In practice the typical neutron polarization was about 70%. The spin direction of the neutrons are reversed rapidly (every ten seconds) by an adiabatic spin flipper [18].

To reduce the effect of Doppler broadening on the resonance line shape, the ^{232}Th target was cooled to 77 K by a liquid-nitrogen target chiller. A natural boron neutron absorber was located at the upstream end of the spin flipper in order to remove low-energy neutrons that would overlap with neutrons from the next pulse.

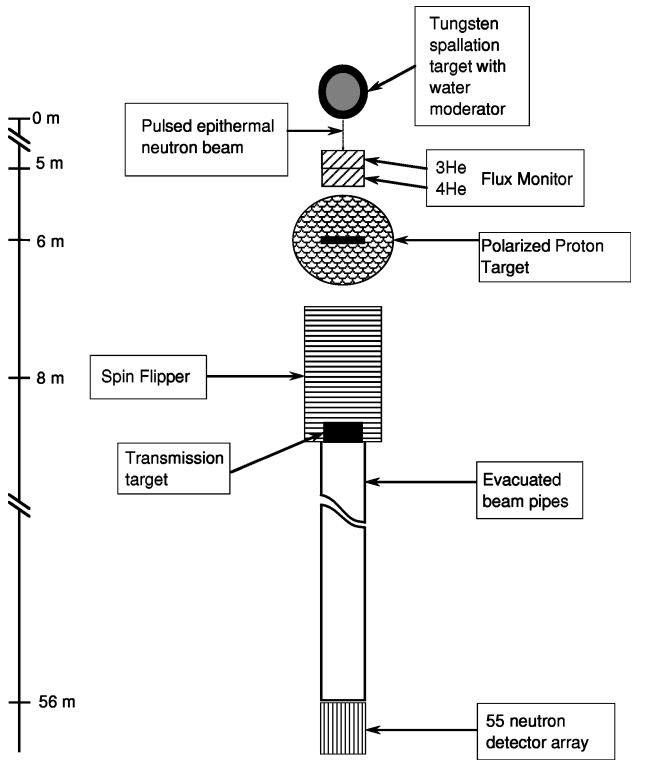

FIG. 1. Overview of TRIPLE polarized neutron flight path at LANSCE.

The neutron detector system consists of 55 liquid scintillator cells optically coupled to photomultipliers (PMT's) [19]. The detector is located 56 m from the neutron source. The segmented nature of the detector allows very high instantaneous counting rates, while the thickness of the scintillator is such that most of the neutrons are thermalized and captured, giving the detector a very high and almost energy-independent efficiency.

B. Data acquisition

The data acquisition cycle is initiated by each proton burst. An inductive pickup on the proton beam line (before the spallation target) provides a time-zero signal t_0, which also triggers a second pulse, t_0' , 1/60th of a second later. The detector signals are linearly summed and filtered to 100, 200, or 1000 ns, with the time depending on the digital sampling interval (dwell time). A digital transient recorder samples the summed detector signal 8192 times in intervals determined by the dwell time, and these 8192 words are added to a summation memory for 200 beam bursts before being stored. The t_0' pulse initiates a sweep 1/60th of a second after each neutron pulse and triggers the subtraction of the next 8192-word sweep from the stored data. Each sweep is thus corrected for background and electronic noise, and this correction is also applied to the monitor signal.

This process is followed for 200 beam bursts (or t_0 pulses). The helicity state of the neutron beam is changed according to an eight-step sequence designed to reduce the effects of gain drifts and residual transverse magnetic fields on the PMT's [13]. Each spin-flipper state lasts 10 s. The data are stored in separate spectra, one for data with the spin unchanged (NOFLIP) and one for data with the spin flipped

(FLIP). After 20 eight-step sequences, the data collection is stopped and the data are stored for later analysis. The result is a rather large number of small data sets, runs, that are analyzed separately.

III. DETERMINATION OF PNC LONGITUDINAL ASYMMETRIES

The code FITXS [20] was written specifically to analyze the time-of-flight (TOF) spectra measured by the TRIPLE Collaboration at MLNSC. For a particular time-of-flight region and a set of fitting parameters, the χ^2 is minimized to obtain the optimum set of parameter values. The fitting function depends on the target areal density, the multilevel cross sections, and broadening due to three sources: the neutron beam, Doppler broadening, and the detector system. The broadening due to the beam and the detection system can be combined to form a response function $B_t(t)$.

For this transmission experiment, the fitting function can be written as

$$\mathcal{F}_t(t)=B_t(t)\otimes[N_0(t)e^{-n\sigma_D(t)}]+\mathcal{B}, \tag{1}$$

where

$$\sigma_D(t)=[D(v)\otimes\sigma(v)]_{v\to t}, \tag{2}$$

$N_0(t)$ is the neutron flux, $D(v)$ is the velocity-dependent Doppler response function, $\mathcal{B}$ is the background function, and the $v\to t$ symbol indicates that after the convolution in velocity space, the function is converted to a function of time. The $\otimes$ symbol indicates a convolution.

The first step in the analysis approach is to fit the neutron cross section data, and then to fix all of the resonance parameters while determining the longitudinal asymmetries. The multilevel, multichannel neutron cross section is calculated with the formalism of Reich and Moore [21].

We adopt the following notation: the resonance energy is $E_{s,p}$, the neutron width $\Gamma_n^{s,p}$, and the total width $\Gamma^{s,p}$, all for s- and p-wave resonances, respectively. Detailed expressions for the s- and p-wave elastic and capture cross sections are given in the preceding paper [1]. The neutron widths are calculated at energy E according to

$$\Gamma_n^{s,p}(E)=\Gamma_n^{s,p}(E_{s,p})[E/E_{s,p}]^{l+1/2}. \tag{3}$$

The details of the fitting procedure are given in the preceding paper [1]. The final expression for $B_t(t)$ includes the beam response and additional broadening from the neutron detector, with the various resolution parameters determined empirically for this system. Including an energy-dependent flux and allowing for background (described by a polynomial in time), the final fitting function can be written as

$$\mathcal{F}_t(t)=\left[B_t(t)\otimes\left[\frac{\alpha}{E^\beta}e^{-n\sigma_D(t)}\right]\right]+\sum_{i=0}^{3}\frac{a_i}{t^i}, \tag{4}$$

where $\sigma_D(t)$ is the Doppler-broadened total cross section for s- and p-wave resonances. The s- and p-wave cross sections are calculated for all resonances present in a TOF spectrum (including contaminants).

When a final satisfactory fit is obtained for a given energy region, all of these parameters are held fixed and the longitudinal asymmetry p varied. This is performed for each helicity state for each run. As described in the introduction, once the cross sections $\sigma_p^{\pm}$ are determined, the PNC longitudinal asymmetries are easily obtained. A detailed description of the code FITXS is given by Matsuda [20].

IV. DATA

The PNC effects in ^{232}Th were studied by transmitting neutrons through a thick sample. The target was a cylinder of natural thorium (^{232}Th) 11.20 cm in length and 9.84 cm in diameter, which corresponds to an areal density of 3.40×10^{23} atoms/cm^2. Preliminary evaluation of the data focused on possible experimental difficulties, including gain fluctuations or large numbers of bad spectra. After these cuts were made, 307 runs were used in the final analysis. The earlier thorium experiment consisted of 355 runs of the same length. In the present experiment the neutron polarization was about 70% rather than the value of 27% obtained in the earlier experiment. In addition, when increased collimation size and detector efficiency are considered, the effective beam intensity in the present experiment is about an order of magnitude higher than in the earlier measurements. Since the standard figure of merit for the beam is P^2I, where P is the beam polarization and I the beam current, the present data should be nearly two orders of magnitude better than the earlier data.

In order to study parity violation at the 8.3-eV resonance, it was essential to collect data at 200-ns dwell time. (For 100-ns dwell time the spectrum would end before 8.3-eV neutrons arrived at the detector.) However, for higher energies the 100-ns dwell time data are preferred, since this channel width provides more data points per resonance, and therefore effectively better resolution. A total of 159 runs with 200-ns dwell time and 148 runs with 100-ns dwell time were included in the final analysis. Resonances below 25 eV are observed only in the 200-ns data; both data sets were used in the energy region 25-234 eV; and above 234 eV only the 100-ns data were analyzed.

The initial energy calibration was performed using previous resonance data [22,23]. For the 100-ns data the time-of-flight length was $L=56.804$ m and the channel offset was $C_0=7.42$ channels, while the corresponding values for the 200-ns data were $L=56.795$ m and $C_0=4.18$ channels.

The statistical error in these values is very small, but the total error is not known since the errors in the resonance energies used to determine L and C_0 were not given in Refs. [22,23]. Using the values of L and C_0 given above, the resonance energies were converted back to time-of-flight channels and related to the Olsen [22] resonance energies by $E=5.23\times10^{-9}[L^2/\delta^2(C+C_0)^2]$, where δ is the dwell time. Assuming that the fractional errors in the thorium measurement by Olsen were the same as in their uranium measurement [24] with the same system, a least-squares fit was performed to determine a new length and a new channel offset. The new length was found to be $L=56.778\pm0.006$ m, with $C_0=7.47\pm0.33$ channels for the 100-ns data. For the 200-ns data $L=56.776\pm0.005$ m and $C_0=3.80\pm0.14$ channels. With this calibration the resonance energies and their errors

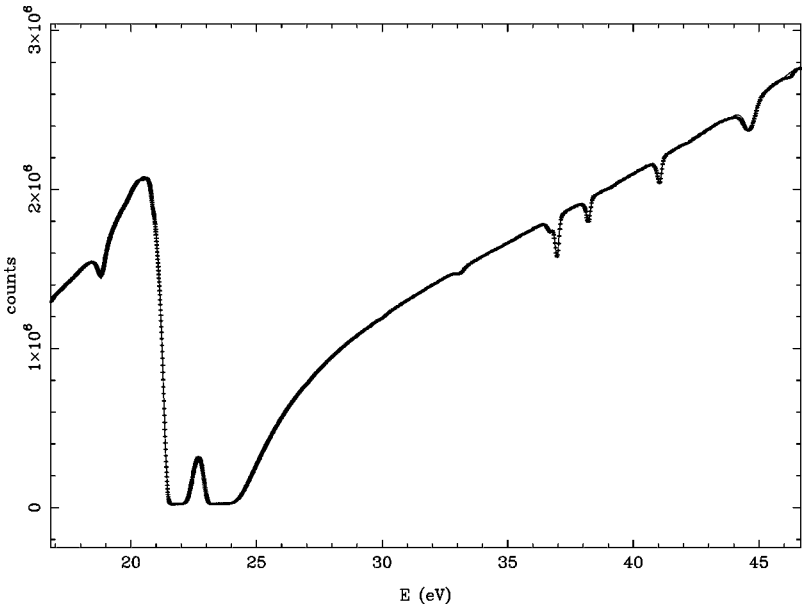

FIG. 2. Sample multilevel fit to a ^{232}Th transmission spectrum in the energy region 16.9–46.5 eV.

were determined. The agreement with the earlier measurements is excellent. Due to the higher statistics of the present measurement, the resonance parameters for the weak p-wave resonances should be more precise. However, since for this experiment the length of the flight path was relatively short, and a rather thick target (optimized for the study of parity violation in weak p-wave resonances, not for resonance analysis) was used, not all known resonances were observed due to overlapping with strong s-wave resonances.

As the final steps in processing the data for analysis, the analog-to-digital converter counts are converted to actual neutron counts, the data are corrected for dead time, and background due to γ-ray counts is subtracted. The dead time is determined from the relation $Y=Re^{-R\tau}$, where Y is the measured yield, R is the actual counting rate, and τ is the dead time. The rates are measured for a typical beam current, and at one-half, one-quarter, and one-eighth of the typical current, and τ is determined. For this measurement the dead time was 23.0 ns. The counts that appear at the bottom of black resonances are assumed to arise from γ rays in the neutron beam. Yen *et al.* [25] developed a procedure to correct for this background. With these corrections, the data are now ready for determination of the neutron resonance parameters.

V. DATA REDUCTION

A. Neutron resonance parameters

In the analysis to determine the resonance parameters, 30 runs were summed for the 100-ns data as well as the 200-ns data as a compromise between better statistics and the maintenance of uniform experimental conditions. Due to the thickness of the thorium target, many of the s-wave resonances absorbed all neutrons. After the standard background correction [25] there were still some counts under these resonances. The remaining counts were fit to a polynomial function of 1/TOF. These background parameters were held fixed for the rest of the fitting process.

The procedure was similar to that described in the preceding paper. First a large energy region was fit with known s-wave resonance parameters, allowing the magnitude and energy dependence of the flux to vary. The energy dependence was then fixed. Then a smaller energy region was fit, allowing E_s, $g\Gamma_n^s$, and Γ_γ^s to vary. This process was then repeated after adding a higher energy region with some additional s-wave resonances. These new resonances were then fit, with the resonance parameters for the first s-wave resonances held fixed. This process was iterated until the s-wave parameters were stable. Then the p-wave resonances were fit while allowing only the flux and the p-wave resonance parameters to vary. The resulting fits were usually very good, as illustrated by a sample fit shown in Fig. 2.

The key issue is over what energy range this analysis procedure is reliable. As the energy increases, the resonances observed in the time-of-flight spectra comprise fewer channels, and the resonance parameters extracted become less well determined. The problems are accentuated for the weaker resonances that are our primary focus. However, as we discuss in detail below, all of the statistically significant PNC effects have the same sign. It therefore would be very interesting to extend the measurements and analysis into this difficult energy region. In an effort to extend the energy range, we have performed measurements using a large solid angle capture detector [26,27]. (Since for these neutron resonances the capture width is nearly equal to the total width, measuring the emitted γ rays provides information equivalent to that obtained via the transmission measurements.) Because the capture detector had no moderation time, and because the capture measurements were made with a different sample, these capture measurements did not significantly extend the energy range for which we have reliable parity violation data. However, the capture measurements do provide an opportunity to test the reliability of the data analysis method. For sample lower energy resonances the widths obtained from the transmission and capture measurements agree, and these widths agree with the literature values. Similarly, our measurements for the PNC longitudinal asymmetries obtained via capture and transmission agree. However, for resonances near 300 eV, the resonance parameters obtained from the two methods do not agree, and the widths

TABLE I. Resonance parameters for ^{232}Th.

E (eV)	BP [a]	l	J [b]	$g\Gamma_n$ (meV)	Γ_γ (meV)	A_i (1/eV)
8.36032±0.0012	1.00	1	0.5	0.000267±0.000004		25.0
13.1377±0.0018	1.00	1		0.000193±0.000004		38.5
21.819±0.003	0.00	0	0.5	2.18±0.044	24.98±0.50	
23.454±0.003	0.00	0	0.5	4.10±0.082	24.16±0.48	
36.982±0.004	0.99	1		0.000882±0.000018		20.5
38.232±0.004	0.99	1	0.5	0.000481±0.00001		27.1
41.066±0.005	0.99	1		0.000510±0.00001		27.0
47.068±0.005	0.99	1	0.5	0.00174±0.000035		17.3
49.941±0.006	0.99	1		0.000429±0.00001		40.0
58.786±0.009	0.98	1		0.00902±0.00018		58.3
59.523±0.009	0.00	0	0.5	3.88±0.083	23.93±0.49	
64.575±0.010	0.99	1	0.5	0.000794±0.000037		103.0
69.228±0.015	0.00	0	0.5	44.52±0.91	20.65±0.56	
90.139±0.01	0.99	1		0.00559±0.00013		11.6
98.057±0.013	0.99	1	0.5	0.00429±0.000098		12.9
103.63±0.01	0.99	1		0.00650±0.00013		13.4
113.00±0.01	0.00	0	0.5	13.07±0.27	23.89±0.52	
120.83±0.02	0.00	0	0.5	22.67±0.47	23.54±0.51	
128.17±0.02	0.89	1	0.5	0.0801±0.0044		13.6
129.16±0.02	0.00	0	0.5	3.59±0.79	27.54±1.10	
145.83±0.02	0.90	1		0.088±0.003		2.89
148.06±0.02	0.99	1		0.0063±0.0001		12.4
154.29±0.02	0.49	0	0.5	0.193±0.015	22.51±0.49	
167.11±0.03	0.98	1	0.5	0.0235±0.0006		33.8
170.30±0.04	0.00	0	0.5	62.23±1.35	22.14±1.18	
178.86±0.03	0.98	1		0.0246±0.0007		15.5
192.60±0.03	0.00	0	0.5	16.36±0.36	23.82±0.48	
196.20±0.03	0.96	1	0.5	0.070±0.002		11.4
199.25±0.03	0.00	0	0.5	9.58±0.19	20.54±0.43	
202.58±0.03	0.98	1	0.5	0.0422±0.002		11.2
210.91±0.03	0.98	1		0.0181±0.0004		10.5
221.11±0.04	0.00	0	0.5	29.25±0.60	23.16±0.47	
231.95±0.04	0.98	1	0.5	0.0102±0.0005		12.6
234.07±0.04	0.98	1		0.0161±0.0004		10.1
242.25±0.04	0.98	1		0.0434±0.0009		7.04
251.47±0.05	0.00	0	0.5	31.05±0.65	26.09±0.81	
263.04±0.05	0.00	0	0.5	21.16±0.50	24.98±0.71	
276.45±0.03	0.98	1		0.0086±0.0002		17.1
285.68±0.06	0.00	0	0.5	30.56±0.76	25.86±1.04	

[a]Bayesian p-wave probability.

[b]$J=0.5$ is assigned to p-wave resonances with statistically significant PNC asymmetries.

obtained for the transmission data do not agree with the literature. The PNC asymmetries determined via transmission and capture (for example for the 302-eV resonance) do not agree. We therefore conclude that for this target our analysis of the transmission data is reliable up to some cutoff energy near 300 eV. After careful examination of the data we have adopted 285 eV as the cutoff value.

The final values for the resonance parameters are given in Table I. The errors on $g\Gamma_n$ and Γ_γ include the statistical uncertainty (which is very small) and an estimated 2% uncertainty from the fitting process. This is an attempt to include systematic uncertainties from the fitting process and from uncertainties in the response function. There is an additional 2% uncertainty included for the p waves due to small fluctuations in the flux. We believe that the uncertainty estimate is conservative. Our central results—the parity violating longitudinal asymmetries—are insensitive to small changes in the resonance parameters.

The measurement determines the value of $g\Gamma_n$, not the value of the orbital angular momentum l. This leaves the possibility that a strong p-wave resonance or a weak s-wave resonance may be misassigned. We used the Bayesian analysis procedure of Bollinger and Thomas [28] to determine the orbital angular momentum of each resonance. The Bayesian analysis uses the measured widths, strength functions, and level densities, and relies mainly on the large difference in s- and p-wave penetrabilities. The procedure is the same as described in detail in the preceding paper. From our neutron

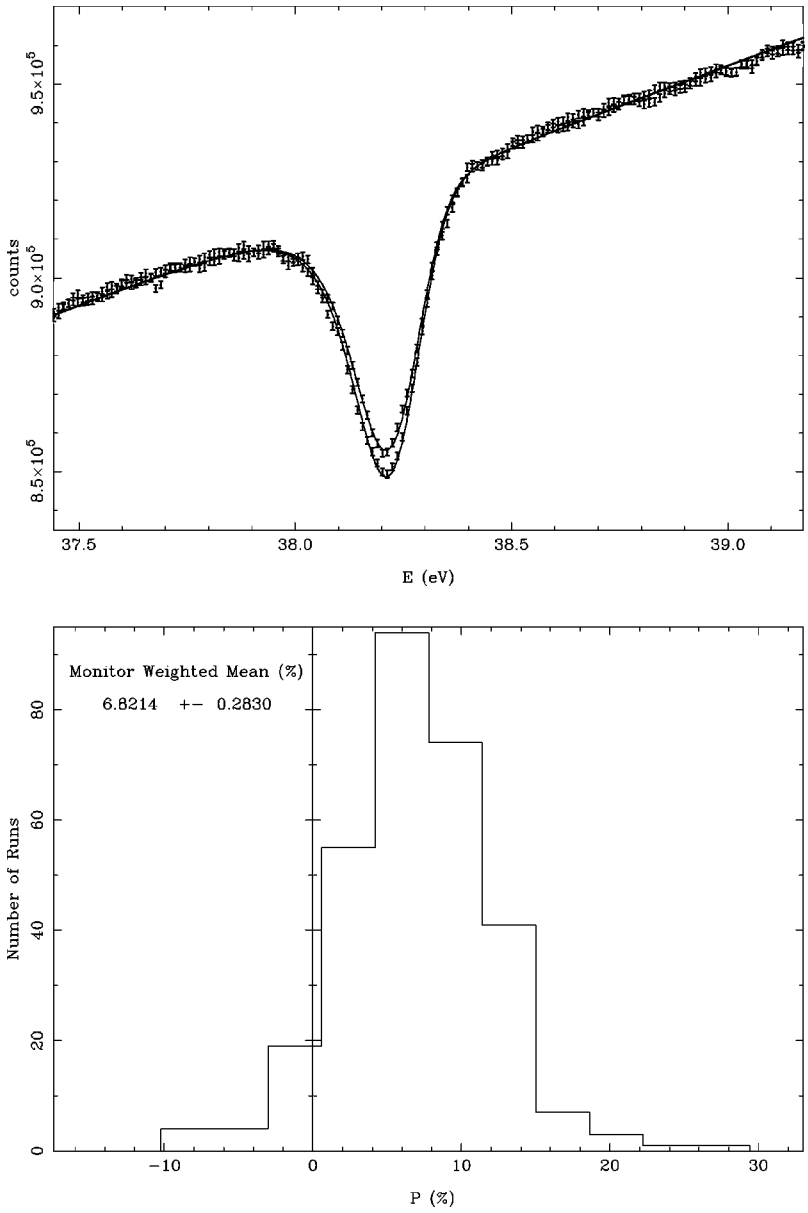

FIG. 3. (top) ^{232}Th transmission spectra for two helicity states near the 38.2-eV resonance. (bottom) Histogram of the asymmetries obtained for each of 150 runs for the resonance shown at the top of the figure.

resonance data we determined the average s-wave level spacing $D_0=(19\pm3)$ eV, and the s- and p-wave strength functions $S_0=(0.9\pm0.3)\times10^{-4}$ and $S_1=(0.8\pm0.2)\times10^{-4}$. Both the s-wave level spacing and strength function agree with previous results, $D_0=(16.8\pm1.0)$ eV and $S_0=(0.84\pm0.07)\times10^{-4}$ [23]. The p-wave strength function calculated for the energy range below 285 eV with the data of Ref. [23] is $S_1=(1.00\pm0.25)\times10^{-4}$. The missing neutron p-wave strength in our measurement is due to the blocking of some p-wave resonances in the transmission spectrum, since a thick sample was used to optimize the PNC study. The large uncertainty in our values is due primarily to the limited energy range of the present work. We have used the level spacing and strength function results of [23] to estimate the probability that a given resonance is a p-wave resonance. This probability is listed for each resonance in Table I. The only disagreement is for the 196.2-eV resonance, which we assign as p-wave rather the earlier s-wave assignment. This resonance shows a very strong parity violation effect, consistent with the Bayesian probability.

B. PNC longitudinal asymmetries

The PNC longitudinal asymmetries were obtained by fitting each run with the code FITXS; the asymmetry parameter was varied while all other parameters were held fixed. The sum of the data for the two helicity states (FLIP + NOFLIP) was fit to determine the flux for a single run. With all other parameters held fixed, the data for each helicity state was fit separately to determine p^+ and p^- for each run. The observed asymmetry p is determined from p^+ and p^-. The neutron polarization was measured for each run. The asymmetries for a sample resonance are shown in Fig. 3. The average p values and their uncertainties were determined separately for each polarization orientation, and these two values combined to obtain the value of the longitudinal asymmetry and its uncertainty for each resonance. These asymmetry values for each resonance are corrected for the spin-flipping efficiency, which depends only on the neutron energy. The final longitudinal asymmetries are shown as a function of energy in Fig. 4 and are listed in Table II.

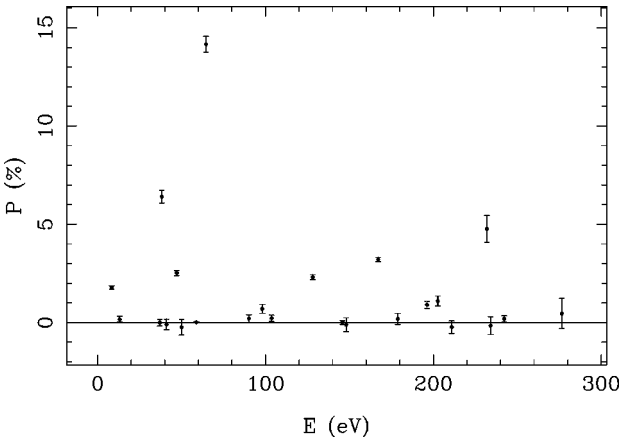

FIG. 4. Longitudinal PNC asymmetries p versus energy E for ^{232}Th.

These new results show a dramatic improvement relative to the results of the earlier measurements [10]. There are now ten PNC effects with a statistical significance of 3 σ or greater. In addition the resonances that show no effects (approximately two-thirds of the p-wave resonances should have $J=3/2$ and cannot display parity violation) have much smaller uncertainties than in the earlier data. The answer to the key question—is the nonstatistical distribution of the signs of the longitudinal asymmetries real or a statistical artifact?—is apparent by inspection. The ten statistically significant effects all have the same sign, which should happen at random only once in 2^{10} or 1024 trials.

TABLE II. PNC asymmetries for ^{232}Th.

E (eV)	p (%)	$p/\Delta p$	$p\sqrt{E}$ $(\%\sqrt{\text{eV}})$
8.36032	1.78±0.09	19.8	5.15
13.1377	0.16±0.14	1.1	0.58
36.982	−0.01±0.17	−0.1	−0.61
38.232	6.41±0.32	20.0	39.6
41.066	−0.09±0.27	−0.3	−0.58
47.068	2.52±0.13	19.4	17.3
49.941	−0.24±0.39	−0.6	−1.70
58.786	0.02±0.03	0.7	0.15
64.575	14.16±0.41	34.5	114.0
90.139	0.21±0.19	1.1	1.99
98.057	0.70±0.22	3.2	6.93
103.63	0.22±0.16	1.4	2.24
128.17	2.31±0.12	19.2	26.1
145.83	0.00±0.10	0.0	0.00
148.06	−0.11±0.34	−0.3	1.34
167.11	3.21±0.10	32.1	41.5
178.86	0.19±0.28	0.7	2.54
196.20	0.90±0.18	5.0	12.6
202.58	1.10±0.25	4.4	15.7
210.91	−0.23±0.32	−0.7	−3.34
231.95	4.77±0.68	7.0	72.6
234.07	−0.16±0.45	−0.4	−0.24
242.25	0.18±0.17	1.0	2.80
276.45	0.46±0.76	0.6	7.65

The average value for the longitudinal asymmetry p is $\overline{p}=1.60\pm0.65\%$ for all analyzed p-wave resonances. If only asymmetries with a statistical significance of greater than 3 σ are considered, the value for $\overline{p}$ increases to $3.8\pm1.3\%$. It is interesting to compare these results with those obtained for ^{238}U [1], where $\overline{p}$ was consistent with zero both for the set of all analyzed p-wave resonances and also for those p-wave resonances with statistically significant parity violations. The value for $\overline{\Delta\sigma}$ is also of interest. For all analyzed p-wave resonances $\overline{\Delta\sigma}=0.29\pm0.14$ b, while for the ten large effects, $\overline{\Delta\sigma}=0.69\pm0.30$ b. These values are larger than those obtained for ^{238}U [1]. However, the average value of $\overline{\Delta\sigma}$ is dominated by one very large contribution (from the 128-eV resonance), which is not the case for the longitudinal asymmetries. We therefore draw no strong conclusions from the value of $\overline{\Delta\sigma}$.

VI. ANALYSIS

A. Method

First we briefly review the analysis adopted in the preceding paper [1], and then discuss the changes required to consider the nonstatistical anomaly. For a target with $I^{\pi}=0^{+}$, the s-wave resonances have $1/2^{+}$ and the p-wave resonances $1/2^{-}$ or $3/2^{-}$. Only $1/2^{-}$ resonances mix with the $1/2^{+}$ resonances to show parity violation. The two-level approximation [29–33] for the observed PNC asymmetry p_{μ} was generalized to include admixtures from a number of s-wave resonances ν [7]

$$p_{\mu}=2\sum_{\nu}\frac{U_{\nu\mu}}{E_{\nu}-E_{\mu}}\frac{g_{\nu_{1/2}}g_{\mu_{1/2}}}{\Gamma_{n}^{\mu}}, \tag{5}$$

where $g_{\mu_{1/2}}$ and $g_{\nu_{1/2}}$ are the neutron decay amplitudes of levels μ and ν ($g_{\mu}^{2}=\Gamma_{n}^{\mu}$ and $g_{\nu}^{2}=\Gamma_{n}^{\nu}$), and $U_{\nu\mu}$ is the matrix element of the PNC interaction between levels ν and μ. The signed quantities $U_{\nu\mu}$, g_{μ}, and g_{ν} are statistically independent random variables with mean-zero Gaussian distributions. Although there is insufficient information to obtain the individual matrix elements, one can determine the *variance* of the distribution of these matrix elements. The common variance M^{2} of the PNC matrix elements is the mean-square matrix element of the PNC interaction.

The quantity p_{μ} is the sum of Gaussian random variables and therefore is itself a Gaussian random variable. The variance of p_{μ} is $M^{2}A_{\mu}^{2}$, where

$$A_{\mu}^{2}=\sum_{\nu}A_{\nu\mu}^{2}\quad\text{and}\quad A_{\nu\mu}^{2}=\left(\frac{2}{E_{\nu}-E_{\mu}}\right)^{2}\frac{\Gamma_{n}^{\nu}}{\Gamma_{n}^{\mu}}. \tag{6}$$

The quantity A_{μ} is listed for each resonance in Table I. A maximum likelihood approach to the analysis was adopted [34,35]. The probability density function (PDF) of the PNC asymmetry p_{μ} is a Gaussian $G(p_{\mu},M^{2}A_{\mu}^{2})$ with mean zero and variance $M^{2}A_{\mu}^{2}$. Including the experimental error σ_{μ} yields a Gaussian PDF with variance $M^{2}A_{\mu}^{2}+\sigma_{\mu}^{2}$

$$G(p_{\mu},M^{2}A_{\mu}^{2}+\sigma_{\mu}^{2}). \tag{7}$$

If all spectroscopic information is known, then the likelihood function for a given p-wave resonance μ is

$$L(M)=G(p_\mu, M^2A_\mu^2+\sigma_\mu^2)P_M(M), \tag{8}$$

where P_M is the *a priori* probability density, p_μ is the experimental value of the PNC asymmetry, and σ_μ is the uncertainty in p_μ.

If the p-wave spins are not known, then the likelihood function is the sum of two terms, with the additional term a Gaussian that is independent of the PNC matrix element M.

$$L(M)=[a(1/2)G(p_\mu, M^2A_\mu^2+\sigma_\mu^2) + b(3/2)G(p_\mu, \sigma_\mu^2)]P_M(M), \tag{9}$$

where a and b are the probabilities that $J=1/2$ or $3/2$. (Since the $p_{1/2}$ and $p_{3/2}$ states have different average strengths, and there is a finite threshold for observability, the number of resonances actually observed does not have the expected statistical ratio. The relative probability is determined empirically—see the discussion by Frankle *et al.* [10].) The justification for this form of the likelihood function is discussed in general by Bowman *et al.* [34] and in detail by Bowman, Lowie, and Sharapov [35].

The *a priori* probability P_M is common to both terms. Since the second term is independent of M, the function is not normalizable without the factor P_M. In practice we assume that P_M is constant up to some maximum value and zero above this value. For a number of independent resonances the likelihood function is the product of the functions for the individual resonances. One inserts the values of the experimental asymmetries p_μ and their uncertainties σ_μ, determines the spectroscopic terms A_μ from the known resonance parameters, and calculates the likelihood function. The location of the maximum gives the most likely value m_L of the parameter M. The confidence interval is obtained by solving the equation

$$\ln\left[\frac{L(m_\pm)}{L(m_L)}\right]=\frac{1}{2}, \tag{10}$$

where $m_\pm$ are the upper and lower values at which this equation is satisfied.

This discussion assumes that the distribution of the asymmetries is a Gaussian with zero mean. This is clearly not true for these data. Since the data appear to obey a statistical distribution about some nonzero value, we represent the data by introducing an offset parameter. Following Bowman *et al.* [7], the asymmetry can be expressed as the sum of two terms: a fluctuating term and a constant term. The expression used is

$$p_\mu=2[\Sigma_\nu U_{\nu\mu}/(E_\nu-E_\mu)](\Gamma_n^\nu/\Gamma_n^\mu)^{1/2}+B[(1\ \text{eV})/E]^{1/2}, \tag{11}$$

where E is in eV. The quantities $U_{\nu\mu}$, E_ν, and E_μ are independent random variables, and the first term has average value zero. The energy dependence of the ratio of widths is $E^{-1/2}$. Expressing the constant term relative to the value at $E_n=1$ eV gives the convenient result that the ratio of the fluctuating and constant terms does not depend on the energy.

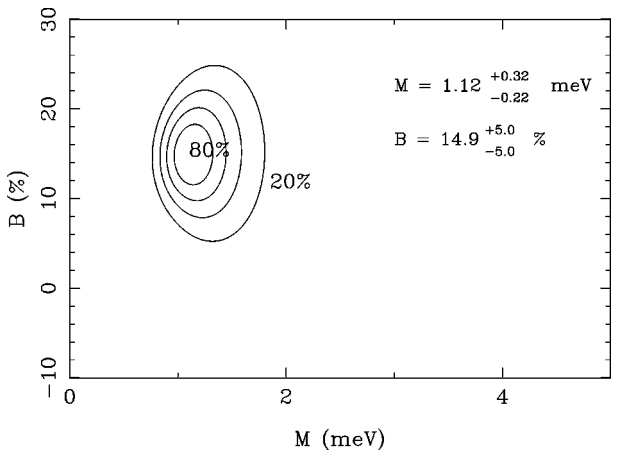

FIG. 5. Two-parameter maximum likelihood plot for ^{232}Th. The curves are contours of constant likelihood, with values 80, 60, 40, and 20 % of the maximum likelihood.

B. Results

We then proceed as before with the maximum likelihood method, except there are now two parameters—the rms PNC matrix element M and the empirical offset B (expressed in %). A two-parameter maximum likelihood plot for the ^{232}Th data is shown in Fig. 5, using $a=0.41$ and $b=0.59$. The values for M and B are $M=1.12^{+0.32}_{-0.22}$ meV and $B=14.9^{+5.0}_{-5.0}$%. For a level spacing $D_0=16.8$ eV [23], this gives a weak spreading width of $\Gamma_w=4.7^{+2.7}_{-1.8}\times10^{-7}$ eV. If one ignores the offset and fits the data with only the one parameter M, the result is $M=1.58^{+0.44}_{-0.31}$ meV. Thus the value of M is changed by about 30% if one ignores the offset.

For comparison, we also treat the ^{238}U data presented in the previous paper [1] in the same manner. A two-parameter maximum likelihood plot for ^{238}U is shown in Fig. 6. The values for M and B are $M=0.65^{+0.23}_{-0.15}$ meV and $B=-1.96^{+2.34}_{-2.31}$%.

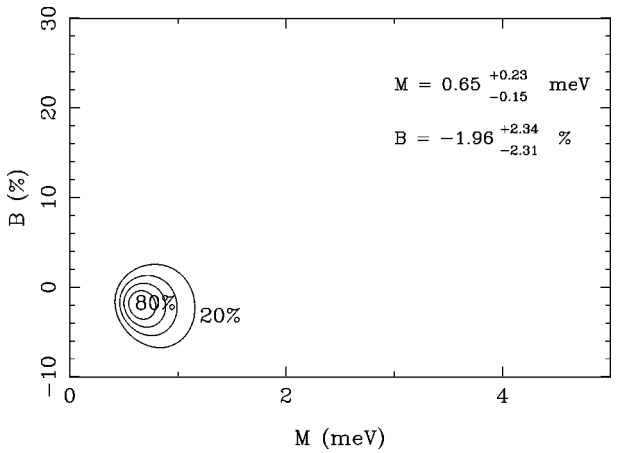

FIG. 6. Two-parameter maximum likelihood plot for ^{238}U. The curves are contours of constant likelihood, with values 80, 60, 40, and 20 % of the maximum likelihood.

VII. SIGN CORRELATION

A. Distant doorway state models

As noted in the previous section, the experimental evidence confirms the earlier measurement. Since ten statistically significant parity violation asymmetries have the same sign, the nonstatistical effect (sign correlation) is confirmed.

Following the original measurement, there were a number of attempts to explain the sign correlation. Both chronologically and in the general physics approach, the explanations divide into two categories. The first set of explanations can be loosely designated as ''distant'' doorway state models. The compound nucleus is by definition very complicated and expected to display random phases. Single particle or doorway state effects were considered first as the origin of the sign correlation. One can express B in terms of doorway states $|d\rangle$ as

$$B=2\sum_d \sqrt{\frac{\Gamma^d_{(n)}}{\Gamma^p_{(n)}}}\frac{\langle 1/2^+ d|V_{PV}|1/2^-\mu\rangle}{(E_\mu-E_d)}. \tag{12}$$

The first explanation was due to Bowman *et al.* [36]. Their approach uses single-particle s- and p-wave states that are located some five MeV away from the p-wave resonances that display parity violation. The influence of the single-particle state does lead to a sign correlation. However, in order to explain the size of the observed effect, the matrix element $\langle d|V_{PV}|\mu\rangle$ must be 100 times larger than all other evidence suggests. This failing—that an unphysically large weak matrix element is required in order to reproduce the size of the nonstatistical effect—proved to be a recurring theme.

Auerbach [37] writes the spreading width due to parity violation as

$$\Gamma_w=\sum_d \Gamma^d_{(n)}\frac{|\langle 1/2^+ d|V_{pv}|1/2^-\mu\rangle|^2}{(E_\mu-E_d)^2+(\Gamma^d/2)^2}. \tag{13}$$

He suggested using the $J=0^-$ spin dipoles as the relevant doorway states. Auerbach and Bowman [38] then combined the spirit of these two ideas [36,37]. The doorway states are the spin dipole giant resonances, and are distant in the sense that they are located several MeV from the p-wave resonances under consideration. Auerbach and Bowman start from the parity-violating asymmetry

$$p_m=2\sum_n \frac{\langle n|V_{PV}|m\rangle}{E_m-E_n}\frac{\gamma_n}{\gamma_m}, \tag{14}$$

which is our original result expressed in their notation, where $|n\rangle$ are s-wave resonances, $|m\rangle$ is one p-wave resonance of interest, and their energies are E_n and E_m. The reduced neutron widths are γ_n and γ_m, which can be written in terms of single-particle amplitudes as

$$\gamma_n=\gamma_s\langle 0^+ s_{1/2}|n\rangle, \tag{15}$$

$$\gamma_m=\gamma_p\langle 0^+ p_{1/2}|m\rangle. \tag{16}$$

The matrix element can then be written as

$$\langle n|V_{PV}|m\rangle=\langle n|D_m\rangle\langle D_m|V_{PV}|m\rangle, \tag{17}$$

which illustrates the role of the doorway state $|D_m\rangle$. Taking into account the spin-dipole nature of the parity-violating potential and using closure, one obtains

$$p_m=\frac{2\gamma_s}{\gamma_p}\langle 0^+ s_{1/2}|V_{PV}|0^+ p_{1/2}\rangle\sum_n \frac{|\langle D_m|n\rangle|^2}{E_m-E_n}. \tag{18}$$

The distribution $|\langle D_m|n\rangle|^2$ has its maximum near the doorway state, has a smooth shape, and is MeV away from the p-wave resonances that are measured. This implies that the sign of the parity-violating asymmetry is fixed for the p-wave resonances $|m\rangle$. However, to explain the size of the observed value of B requires a parity-violating matrix element at least two orders of magnitude greater than considered reasonable.

Flambaum [39] used a valence model approach in which the neutron interacts near the nuclear surface. He transformed the weak Hamiltonian into its surface form and calculated the valence component. In this description the inelastic excitations in the target enhance the PNC matrix element. However, again the magnitude of the matrix element must be unreasonably large in order to explain the size of the observed effect.

The optical model was employed by Koonin *et al.* [40] and by Carlson and Hussein [41] and Carlson *et al.* [42] in efforts to explain the sign effect. The optical model was used for the strong parity-conserving part and the weak parity-nonconserving term obtained from perturbation theory. The two groups use different choices of the optical potential. Both results require a PNC matrix element at least 100 times too large.

Lewenkopf and Weidenmüller [43] utilized a single-particle approach with an enhancement of the weak parity-violating matrix element due to an effect called barrier penetration enhancement that results when the neutron (via the strong interaction) is in a virtual p-wave resonance channel. This highly excited p-wave state is MeV above threshold. They use single-particle states as doorways. The combination of the doorways and the barrier enhancement effect leads to a sign correlation. However, in order to explain the size of the effect requires a matrix element that is two orders of magnitude larger than considered reasonable.

Auerbach and Spevak [44] adopted a projection operator approach and used a one-body form for both the parity-violating part of the potential and the strong interaction part. The doorway states are spin-dipole resonances. They numerically evaluated the barrier enhancement term proposed by Lewenkopf and Weidenmüller. Again they required a matrix element that is two orders of magnitude too large.

At this stage it was clear that the distant state approach did not work. This had important implications: if the sign correlation is a general effect and not some specific nuclear structure effect, then a serious problem results. Therefore attention turned to different models which were specific rather than general.

B. Local doorway state models

The difficulty with the distant doorway state models was simply that the energy separation between the p-wave reso-

nances and the doorway was so great that an unphysically large matrix element was required in order to provide an effect of the magnitude observed experimentally. This problem can be removed by assuming a local or nearby doorway. However, now the solution to the problem generates a new problem. Single-particle states and spin dipole states are known to exist, and there are reasonable estimates for their locations and widths. Such guidance is lacking in establishing the physical origin of the local doorways. Some efforts have focused on the special properties of the nuclide ^{232}Th, while others simply postulate the existence of a doorway with convenient features without detailed specifications concerning its origin.

The general spirit is illustrated by the approach of Auerbach *et al.* [45]. Assume a p-wave resonance labeled $|r\rangle$ with escape amplitude γ_r and a doorway d. The longitudinal asymmetry is

$$p \sim -2 \sum_d \frac{(E_r - E_d)\langle d|V_{PV}|r\rangle \gamma_d}{[(E_r - E_d)^2 + \Gamma_d^2/4]\gamma_r}. \tag{19}$$

Assume the doorway is 50 eV from the p-wave resonance of interest and has a width Γ_d of 100 eV. Then for a typical ratio of penetrabilities for γ_d/γ_r of 10^3, one obtains a matrix element of a few meV. Thus the inconsistency is removed and the problem is shifted to the origin and characteristics of the doorway state.

The doorway states in this approach are intermediate structure resonances, assumed not to overlap, and to have spacings intermediate between single-particle and compound nuclear states. Since the striking nuclear structure feature of ^{233}Th is its octupole deformation [46,47], it was only natural to consider this property. Intermediate structure resonances have been observed in ^{233}Th via neutron-induced fission, and have widths and spacings of the same order of magnitude as required in the local doorway approach. Auerbach and Bowman postulate the doorway as occurring in the third well, where the so-called parity doublets nearly coincide. Flambaum and Zelevinsky [48] and Auerbach *et al.* [49] discuss the effects of the octupole doublets. They conclude that the idea is attractive but physically unlikely. Desplanques and Noguera [50] explicitly consider the octupole doublet or third well approach to be very unlikely. As a speculation they suggest that if the nucleus had a nonzero value of $\vec{\sigma}\cdot\vec{p}$, then suppression factors that enter in the usual case do not appear. Desplanques and Noguera also provide a detailed general description of various possible outcomes given different widths and locations of the doorways. All of these considerations emphasize the need for additional parity-violation data on ^{232}Th, in order to constrain the characteristics of the local doorway, whatever its origin.

In another local doorway approach—by Hussein, Kerman, and Lin [51]—the doorway is a standard two-particle–one-hole (2p-1h) state which happens by chance to be located near the p-wave resonances in question. This doorway couples at random to the compound nuclear states and has nothing directly to do with the shape of the thorium nucleus. The general role of doorways in such symmetry-breaking studies is discussed at length by Feshbach, Hussein, and Kerman [52]. In fact they say that this measurement of the sign correlation in thorium may in fact be the first direct evidence for 2p-1h doorways. Unfortunately their approach provides no specific guidelines for the circumstances under which such nonstatistical effects should occur—the effect is almost random.

To summarize, the present status of the sign correlation is that there is no generally accepted explanation for the physical origin of the effect. The simplest explanation involves some local doorway state, but no convincing specific physical argument for the doorway has been presented. There is evidence that the sign correlation does not occur elsewhere. The results for ^{238}U are consistent with a random sign for the PNC longitudinal asymmetries. Preliminary evidence from other measurements by our group on ^{107}Ag, ^{109}Ag, and ^{115}In by Lowie [53], on ^{113}Cd by Seestrom *et al.* [54], on ^{121}Sb, ^{123}Sb, and ^{127}I by Matsuda [20], and on ^{105}Pd and ^{117}Sn by Smith *et al.* [55] all indicate that the signs of the PNC asymmetries are random. Thus, the sign correlation appears to be a real and localized effect that has not yet been explained.

VIII. SUMMARY

PNC longitudinal asymmetries have been measured for 24 p-wave resonances in ^{232}Th. Ten resonances show parity violations with greater than 3.2 σ statistical significance. This is the largest sample ever measured for a single nuclide. The new apparatus provided greatly improved data quality as compared with the initial study, while confirming the qualitative conclusions of the earlier measurements. The analysis method also has been significantly improved. The value of the rms PNC matrix element is $M = 1.12^{+0.32}_{-0.22}$ meV, while the value of the offset is $B = 14.9^{+5.0}_{-5.0}\%$. For an average level spacing $D_0 = 16.8$ eV, this leads to a weak spreading width of $\Gamma_w = 4.7^{+2.7}_{-1.8} \times 10^{-7}$ eV.

The surprising result of the sign correlation has been confirmed: ten successive statistically significant PNC asymmetries have the same sign and the value of $\overline{p}$ is not zero. Numerous proposed explanations for this nonstatistical effect were reviewed, none of which provide a compelling explanation for the effect. Our other measurements (to be discused in future publications) have focused on the $A \approx 100$ mass region near the $3p$ neutron strength function maximum.

ACKNOWLEDGMENTS

This work was supported in part by the U.S. Department of Energy, Office of High Energy and Nuclear Physics, under Grants Nos. DE-FG02-97-ER41042 and DE-FG02-97-ER41033, and by the U.S. Department of Energy, Office of Energy Research, under Contract No. W-7405-ENG-36.

[1] B. E. Crawford *et al.*, Phys. Rev. C **58**, 1225 (1998), the preceding paper.
[2] E. G. Adelberger and W. C. Haxton, Annu. Rev. Nucl. Part. Sci. **35**, 501 (1988).
[3] V. P. Alfimenkov, S. B. Borzakov, Vo Van Thuan, Y. D. Mareev, L. B. Pikelner, A. S. Khrykin, and E. I. Sharpov, Nucl. Phys. **A398**, 93 (1983).
[4] J. D. Bowman, G. T. Garvey, Mikkel B. Johnson, and G. E. Mitchell, Annu. Rev. Nucl. Part. Sci. **43**, 829 (1993).
[5] C. M. Frankle, S. J. Seestrom, N. R. Roberson, Yu. P. Popov, and E. I. Sharapov, Phys. Part. Nuclei **24**, 401 (1993).
[6] V. V. Flambaum and G. F. Gribakin, Prog. Part. Nucl. Phys. **35**, 423 (1995).
[7] J. D. Bowman *et al.*, Phys. Rev. Lett. **65**, 1192 (1990).
[8] X. Zhu *et al.*, Phys. Rev. C **46**, 768 (1992).
[9] C. M. Frankle *et al.*, Phys. Rev. Lett. **67**, 564 (1991).
[10] C. M. Frankle *et al.*, Phys. Rev. C **46**, 778 (1992).
[11] S. L. Stephenson, Ph.D. thesis, North Carolina State University, 1996.
[12] P. W. Lisowski, C. D. Bowman, G. J. Russell, and S. A. Wender, Nucl. Sci. Eng. **106**, 208 (1990).
[13] N. R. Roberson *et al.*, Nucl. Instrum. Methods Phys. Res. A **326**, 549 (1993).
[14] J. J. Szymanski *et al.*, Nucl. Instrum. Methods Phys. Res. A **340**, 564 (1994).
[15] S. I. Penttilä, J. D. Bowman, P. P. J. Delheij, C. M. Frankle, D. G. Haase, R. Mortensen, H. Postma, S. J. Seestrom, and Yi-Fen Yen, in *Time Reversal Invariance and Parity Violation in Neutron Resonances*, edited by C. R. Gould, J. D. Bowman, and Yu. P. Popov (World Scientific, Singapore, 1994), p. 198.
[16] S. I. Penttilä, J. D. Bowman, P. P. J. Delheij, C. M. Frankle, D. G. Haase, H. Postma, S. J. Seestrom, and Yi-Fen Yen, in *High Energy Spin Physics*, edited by K. J. Heller and S. L. Smith, AIP Conf. Proc. No. 343 (AIP, New York, 1995), p. 532.
[17] V. W. Yuan *et al.*, Phys. Rev. C **44**, 2187 (1991).
[18] J. D. Bowman, S. I. Penttilä, and W. B. Tippens, Nucl. Instrum. Methods Phys. Res. A **369**, 195 (1996).
[19] Yi-Fen Yen *et al.*, in *Time Reversal Invariance and Parity Violation in Neutron Resonances* [15], p. 210.
[20] Y. Matsuda, Ph.D. thesis, Kyoto University, 1998.
[21] C. W. Reich and M. S. Moore, Phys. Rev. **111**, 929 (1958).
[22] D. K. Olsen, R. W. Ingle, and J. L. Portney, Nucl. Sci. Eng. **82**, 289 (1982).
[23] S. F. Mughabghab, M. Divadeenam, and N. E. Holden, *Neutron Cross Sections* (Academic, New York, 1988), Vol. 1, Pt. B.
[24] D. K. Olsen, G. de Sausseure, R. B. Perez, F. C. Defilippo, R. W. Ingle, and H. Weaver, Nucl. Sci. Eng. **69**, 202 (1979).
[25] Yi-Fen Yen, J. D. Bowman, L. Y. Lowie, Y. Masuda, G. E. Mitchell, and S. I. Penttilä, Nucl. Instrum. Methods Phys. Res. A **397**, 365 (1997).
[26] C. M. Frankle, J. D. Bowman, S. J. Seestrom, N. R. Roberson, and E. I. Sharapov, in *Time Reversal Invariance and Parity Violation in Neutron Resonances* [15], p. 204.
[27] B. E. Crawford *et al.*, in *IV International Seminar on Interactions of Neutrons with Nuclei* (JINR, Dubna, 1997), p. 268.
[28] L. M. Bollinger and G. E. Thomas, Phys. Rev. **171**, 1293 (1968).
[29] O. P. Sushkov and V. P. Flambaum, Pis'ma Zh. Eksp. Teor. Fiz. **32**, 377 (1980) [JETP Lett. **32**, 352 (1980)].
[30] V. E. Bunakov and V. P. Gudkov, Z. Phys. A **303**, 285 (1981).
[31] V. P. Alfimenkov, Usp. Fiz. Nauk **144**, 361 (1984) [Sov. Phys. Usp. **27**, 797 (1984)].
[32] J. R. Vanhoy, E. G. Bilpuch, J. F. Shriner Jr., and G. E. Mitchell, Z. Phys. A **331**, 1 (1988).
[33] C. R. Gould, D. G. Haase, N. R. Roberson, H. Postma, and J. D. Bowman, Int. J. Mod. Phys. A **5**, 2181 (1990).
[34] J. D. Bowman, L. Y. Lowie, G. E. Mitchell, E. I. Sharapov, and Yi-Fen Yen, Phys. Rev. C **53**, 285 (1996).
[35] J. D. Bowman, L. Y. Lowie, and E. I. Sharapov, Phys. Part. Nuclei **27**, 398 (1996).
[36] J. D. Bowman, G. T. Garvey, C. R. Gould, A. C. Hayes, and M. B. Johnson, Phys. Rev. Lett. **68**, 780 (1992).
[37] N. Auerbach, Phys. Rev. C **45**, R415 (1992).
[38] N. Auerbach and J. D. Bowman, Phys. Rev. C **46**, 2582 (1992).
[39] V. V. Flambaum, Phys. Rev. C **45**, 437 (1992).
[40] S. E. Koonin, C. W. Johnson, and P. Vogel, Phys. Rev. Lett. **69**, 1163 (1992).
[41] B. V. Carlson and M. S. Hussein, Phys. Rev. C **47**, 376 (1993).
[42] B. V. Carlson, M. S. Hussein, A. K. Kerman, and C.-Y. Lin, Phys. Rev. C **52**, R11 (1995).
[43] C. H. Lewenkopf and H. A. Weidenmüller, Phys. Rev. C **46**, 2601 (1992).
[44] N. Auerbach and V. Spevak, Phys. Rev. C **50**, 1456 (1994).
[45] N. Auerbach, J. D. Bowman, and V. Spevak, Phys. Rev. Lett. **74**, 2638 (1995).
[46] J. Blons, C. Mazur, D. Paya, M. Ribrag, and H. Weigmann, Nucl. Phys. **A414**, 1 (1984).
[47] J. Blons, Nucl. Phys. **A502**, 121c (1989).
[48] V. V. Flambaum and V. G. Zelevinsky, Phys. Lett. B **350**, 8 (1995).
[49] N. Auerbach, V. V. Flambaum, and V. Spevak, Phys. Rev. Lett. **76**, 4316 (1996).
[50] B. Desplanques and S. Noguera, Nucl. Phys. **A598**, 139 (1996).
[51] M. S. Hussein, A. K. Kerman, and C.-Y. Lin, Z. Phys. A **351**, 30 (1995).
[52] H. Feshbach, M. S. Hussein, and A. K. Kerman, in *Parity and Time Reversal Violation in Compound Nuclear States and Related Topics*, edited by N. Auerbach and J. D. Bowman (World Scientific, Singapore, 1996), p. 157.
[53] L. Y. Lowie, Ph.D. thesis, North Carolina State University, 1996.
[54] S. J. Seestrom *et al.*, Phys. Rev. C (submitted).
[55] D. A. Smith *et al.* (unpublished).